Croatian Society for Materials Protection

Metalurgija/Metallurgy

Vol. 65 No. 4 / 2026

Effect of Cooling Rate on the Precipitation Behavior of MnS Inclusions in 46MnVS5 Non-Quenched and Tempered Steel

H.K. Sun [1], Y.H. Li [2], P. J. Li [3], S.H. Wang [1], B. X. Lu [4], and Y.K. Xue [1,*]

https://doi.org/10.64486/m.65.4.1

[1] Metallurgy and Energy College, North China University of Science and Technology, Tangshan, China
[2] Key Laboratory of lntelligent Equipment Digital Design and Process Simulation, Tangshan University, Tangshan, China
[3] HBIS Group Shisteel Company, Shijiazhuang, China
[4] Tangshan Iron and Steel Group Co., Ltd. Technology Research and Development Center, Tangshan, China
* Correspondence: e-mail: xueyuekai965@163.com

Type of the Paper: Article
Received: October 25, 2025
Accepted: February 2, 2026

Abstract: This study systematically investigated the effects of cooling rates on the morphology, size, distribution, and microstructural properties of MnS inclusions in 46MnVS5 non-quenched and tempered steel through three cooling methods: water quenching, air quenching, and furnace cooling. Results indicate that cooling rate significantly regulates MnS precipitation behavior: under furnace cooling, MnS forms coarse particles that aggregate along grain boundaries, leading to reduced properties; air cooling produced spherical or short rod-shaped MnS with uniform distribution and optimal comprehensive properties; water cooling resulted in fine, dispersed MnS with a martensite/bainite microstructure, enhancing toughness but requiring tempering treatment. A nonlinear relationship between cooling rate and average MnS diameter was established, providing theoretical support for optimizing air cooling processes.

Keywords: non quenched and tempered steel; cooling rate; MnS inclusions; microstructure

1. Introduction

Non-quenched and tempered steels have gained widespread application in automotive and mechanical manufacturing due to their excellent energy efficiency, low cost, and good machinability [1-4]. Medium-carbon microalloyed non-quenched and tempered steels (such as the typical grade 46MnVS5) achieve a favorable balance between strength and toughness through precipitation strengthening and microstructure control, emerging as a key development direction for high-performance forged steels [5-8]. However, the MnS inclusions commonly present in such steels significantly impact material processing properties, toughness, and fatigue life due to their morphology, size, and distribution characteristics. These inclusions represent one of the key factors limiting their further engineering applications [9-11].

Cooling rate is a core process parameter governing MnS precipitation behavior and microstructural evolution in steel [12-15]. Studies indicate that rapid cooling effectively suppresses MnS growth and segregation, promoting its fine and dispersed distribution; conversely, slow cooling facilitates MnS coarsening and aggregation along grain boundaries or dendrites, thereby exacerbating anisotropy in material mechanical properties [16, 17]. Furthermore, cooling rate influences the material's ultimate comprehensive properties by affecting sec-

ondary dendrite average spacing (SDAS) and the type of phase transformation microstructure. Although previous studies have examined the impact of cooling regimes on inclusion behavior, in-depth quantitative research remains scarce regarding the evolution patterns of MnS in non-quenched-and-tempered steels across a wide cooling rate range, as well as the systematic correlation between these patterns and microstructure-mechanical properties [18].

For this purpose, this study selected 46MnVS5 non-quenched and tempered steel as the research subject. Systematic experimental investigations were conducted on three typical cooling processes: water cooling (~60.47 K/s), air cooling (~8.14 K/s), and furnace cooling (~1.13 K/s), corresponding to high, medium, and low cooling rates, respectively [19, 20]. Water quenching is suitable for small-section or thin-walled components (e.g., connecting rods) requiring high strength-toughness balance, achieving MnS refinement and microstructural refinement. Air cooling, the most common post-forging cooling method, is widely used for medium-section parts (e.g., crankshafts), effectively suppressing excessive MnS coarsening while maintaining favorable strength-toughness matching. furnace cooling is predominantly used for large or complex forgings to reduce thermal stresses and improve machinability, though it often results in significant MnS coarsening. By systematically investigating microstructural and MnS inclusion characteristics under different cooling regimes, combined with optical microscopy (OM), scanning electron microscopy (SEM), and the Aspex automated inclusion analysis system, we characterized the variation in MnS morphology, size distribution, and number density with cooling rate. Further correlations were established between secondary dendrite spacing and microstructural analysis to elucidate the intrinsic mechanism by which cooling rate influences MnS distribution and its synergistic evolution with microstructure. Ultimately, a quantitative relationship model linking cooling rate to average MnS size was developed, aiming to provide theoretical and experimental basis for process control and performance optimization of MnS inclusions in non-quenched-and-tempered steels.

2. Test Method

2.1. Experimental raw materials and equipment

The test steel was sourced from industrially produced 46MnVS5 non-quenched and tempered steel continuous cast billets (200×200 mm), with specific chemical composition as shown in Table 1. After cutting and grinding the cast billets, 300 g were precisely weighed using an electronic balance for testing.

The experiment employed an HLLG1217 vertical high-temperature tube furnace with a rated voltage of 380 V for melting and cooling. This equipment operates at a maximum working temperature of 1700 °C and can perform the entire heat treatment process under a high-purity argon protective atmosphere. The experimental setup is shown in Figure 1.

Table 1. Experimental steel composition /wt.%.

C	Mn	Al	Si	P	S	V	N
0,45	1,3	0,009	0.5	0,015	0,025	0,14	0,013

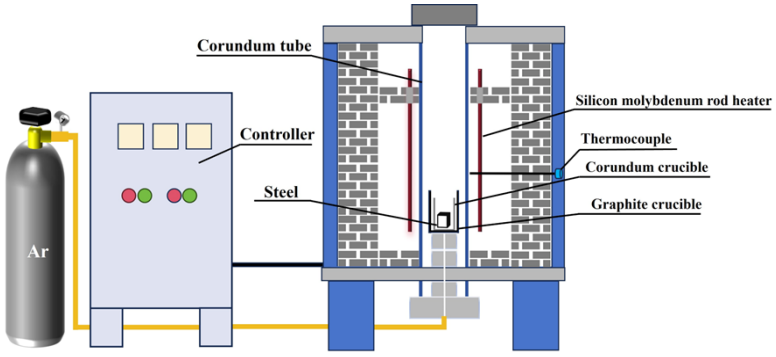

Figure 1. The test equipment is shown in the figure below

 https://doi.org/10.64486/m.65.4.1

2.2. Test steps

The test employed a composite crucible system consisting of an alumina crucible as the inner liner and a graphite crucible as the outer shell. Pre-treated specimens were placed within the alumina crucible before being loaded together into a high-temperature tube furnace. This dual-crucible structure effectively suppresses high-temperature molten steel splashing. After loading, high-purity argon gas was first introduced to displace air within the furnace. Heating proceeded at a rate of 0.0833 °C/s to 1600 °C, followed by a 30-minute soak at this temperature to ensure thorough and uniform melting of the specimens. Upon completion of melting, three distinct cooling processes were applied:

1) Furnace cooling: After holding, the program was terminated. Samples remained in the furnace and were removed using crucible tongs only after cooling to room temperature under argon protection. The average cooling rate from 1600 °C to 800 °C was 1.13 K/s.

2) Air cooling: After holding, carefully remove the corundum crucible with crucible tongs, ensuring safety and avoiding vibration. Place it on a refractory brick to cool naturally in air to room temperature. The average cooling rate from 1600 °C to 800 °C was 8.14 K/s.

3) Water cooling: After holding, carefully remove the corundum crucible using crucible tongs, ensuring safety and avoiding vibration. Place it directly into a container holding 20 L of water (25 °C). Wear protective gear and allow it to cool to room temperature before removing the sample. The average cooling rate from 1600 °C to 800 °C is 60.47 K/s.

The heat treatment process is shown in the curve diagram in Figure 2.

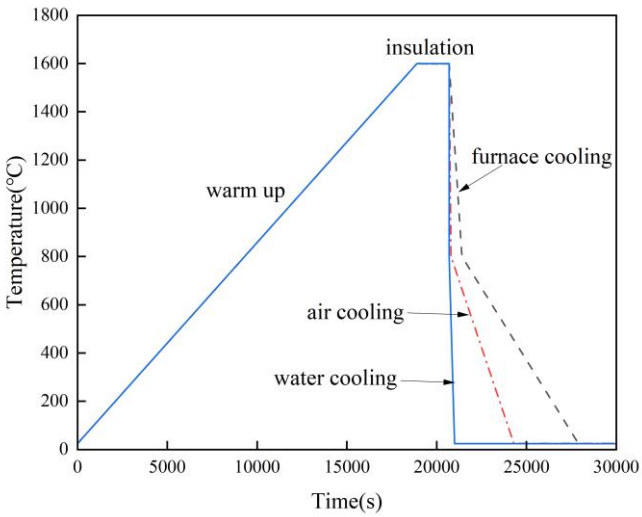

Figure 2. Heat treatment process curve diagram

After the specimen cooled, a wire saw was used to cut a 10 mm × 10 mm × 10 mm cubic metallographic specimen from the center section. The specimen was sequentially ground using 600- to 2000-grit sandpaper. One side of the cube was selected as the working surface and polished with velvet polishing cloth. First, an optical microscope (OM) was used for microstructure observation and image acquisition. Subsequently, combine scanning electron microscopy (SEM-Scios03040702) with energy dispersive spectroscopy (EDS) for morphological observation and compositional identification of MnS inclusions; Further statistical characterization of each specimen was performed using the Aspex-Expex automated inclusion analysis system. Parameters included: gray-scale threshold (70 % – 80 % of matrix gray-scale), size range 0.3 μm – 30 μm, detection area ≥16 mm^2, and acquisition time per particle 200 ms. Classification rule: IF (S > 10 at.%) and (Mn > 10 at.%) then "MnS", enabling systematic acquisition of MnS inclusion size, morphology, and distribution parameters. Finally, sam-

 https://doi.org/10.64486/m.65.4.1

ples were etched for 60 s using a 4 % nitric acid-alcohol solution, rinsed with alcohol, air-dried, and photographed via scanning electron microscopy. Image software was employed to measure secondary dendrite arm spacing (SDAS), establishing a quantitative relationship with cooling rate.

3. Analysis of experiment results

3.1. Morphology, size distribution and quantity of MnS inclusions

The morphology and spatial distribution of MnS inclusions in non quenched and tempered steel under different cooling processes (water cooling, air cooling, furnace cooling) were observed under optical microscope (OM), and the results are shown in Figure 3.

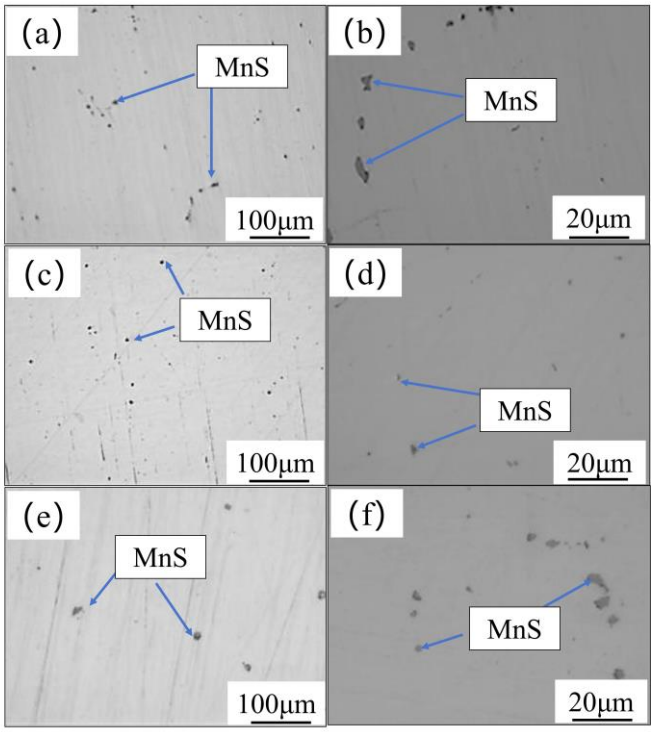

(a),(b).Furnace cooling; (c),(d).Air cooling; (e),(f).Water cooling

Figure 3. Morphology and distribution of sulfides at different cooling rates

As shown in Figure 3 (a) and (b), under the furnace cooling condition, the low cooling rate promotes the full diffusion and growth of MnS inclusions, forming the morphology of coarse size and uneven distribution, and some inclusions precipitate along the grain boundary, which is easy to lead to the decline of impact toughness and fatigue life of steel. Under the air cooling conditions shown in Figures (c) and (d), the size of MnS inclusions is between furnace cooling and water cooling, and the distribution is relatively uniform without obvious aggregation. Moderate cooling rate can effectively inhibit the excessive growth of MnS, and avoid the dispersion segregation caused by rapid cooling, which is helpful to obtain better comprehensive mechanical properties of steel. In addition, MnS is mostly spherical or short rod-shaped under air cooling, which has little adverse effect on the plasticity and toughness of the matrix, so it can be regarded as a compromise cooling method that takes into account the microstructure and properties and process feasibility. However, under water-cooled conditions (Figure (e) and (f)), the higher cooling rate significantly inhibited the diffusion and coarsening of MnS, resulting in a dispersion morphology of fine size and uniform distribution. Such fine and dispersed inclusions help to improve the impact toughness of steel, reduce the formation of crack sources, and improve the strength and fatigue resistance of materials.

https://doi.org/10.64486/m.65.4.1

Comprehensive analysis shows that compared with furnace cooling and water cooling processes, the size of MnS inclusions under air cooling conditions is relatively small. The main reason is that the moderate cooling rate provided by air cooling can not only suppress the sufficient diffusion of Mn and S elements during the solidification process, limit the growth time of sulfides, but also avoid compositional fluctuations and local segregation caused by rapid cooling, thereby allowing MnS to precipitate uniformly in smaller sizes. In contrast, the furnace cooling conditions are similar to the equilibrium solidification process, where Mn and S atoms have sufficient diffusion time to promote the continuous growth of MnS inclusions after nucleation, ultimately forming coarse structures. Under water-cooled conditions, the extremely high cooling rate leads to an increase in the undercooling of the melt. Although the overall composition is uniform, Mn and S elements are prone to transient enrichment at the front of the solid-liquid interface during rapid solidification, causing local concentration supersaturation and resulting in the concentrated precipitation of large-sized MnS inclusions at specific locations.

A comparative analysis of the number density and size distribution of MnS inclusions under three cooling methods—furnace cooling, air cooling, and water cooling—was conducted using the Aspex-Expre automatic inclusion analysis system. The results are shown in Figure 4.

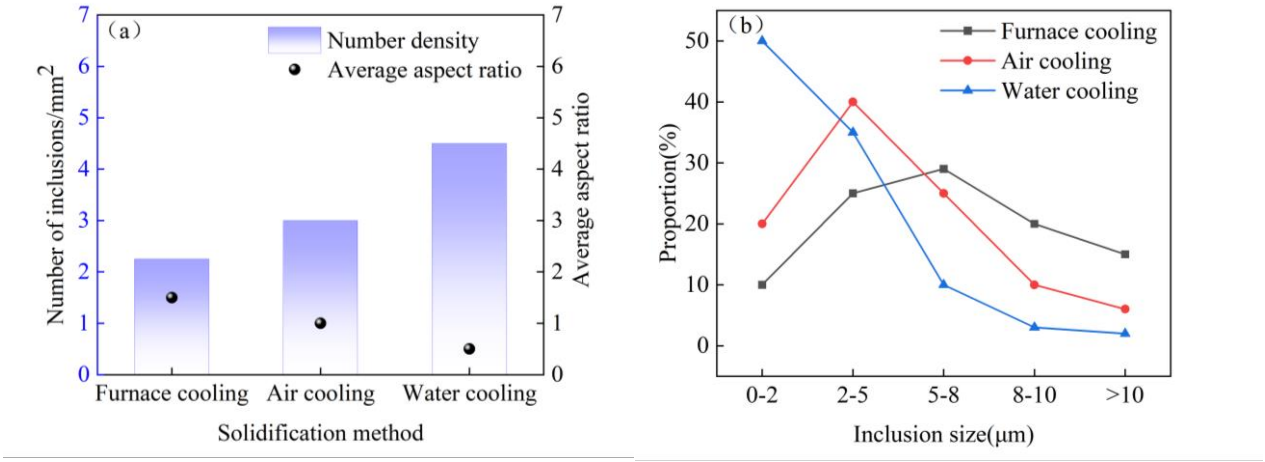

(a). Number density and average aspect ratio of inclusions; (b). Size distribution of inclusions

Figure 4. The influence of different cooling methods on the morphology, number density, and size distribution ratio of MnS inclusions

From Figure 4, it can be seen that as the cooling rate increases, the number density of MnS inclusions significantly increases, and the average aspect ratio significantly decreases. Its shape gradually transitions from a long strip shape under furnace cooling conditions to a short rod-shaped shape under air cooling conditions and a nearly spherical shape under water cooling conditions. Under the condition of furnace cooling (~1.13 K/s), the aspect ratio of MnS inclusions is the highest (about 2.8), with a large proportion of large-sized inclusions (>8 μm) and the lowest number density (about 2.0/mm^2), indicating that slow cooling provides sufficient growth and directional growth conditions for MnS. Under the condition of air cooling (~8.14 K/s), the size of MnS is mainly distributed in the range of (2–5) μm, with an aspect ratio reduced to about 2.0 and a moderate number density (about 3.5/mm^2), exhibiting good size uniformity and distribution consistency, which helps to achieve a balance between the mechanical and processing properties of steel. Under the condition of water cooling (~60.47 K/s), the aspect ratio of MnS is further reduced to about 1.5, and the proportion of small-sized inclusions (0–2) μm is close to 60 %, with the highest number density (about 6.5 mm^{-2}), showing the effective suppression and dispersion effect of rapid cooling on MnS growth, which is conducive to improving the toughness and fatigue resistance of the material.

https://doi.org/10.64486/m.65.4.1

3.2. The influence of sulfide distribution in steel on microstructure

The specimen was etched for 60 seconds using a 4 % nitric acid-alcohol solution, then rinsed with alcohol. After air-drying, scanning electron microscopy was employed to capture the microstructure morphology, as shown in Figure 5.

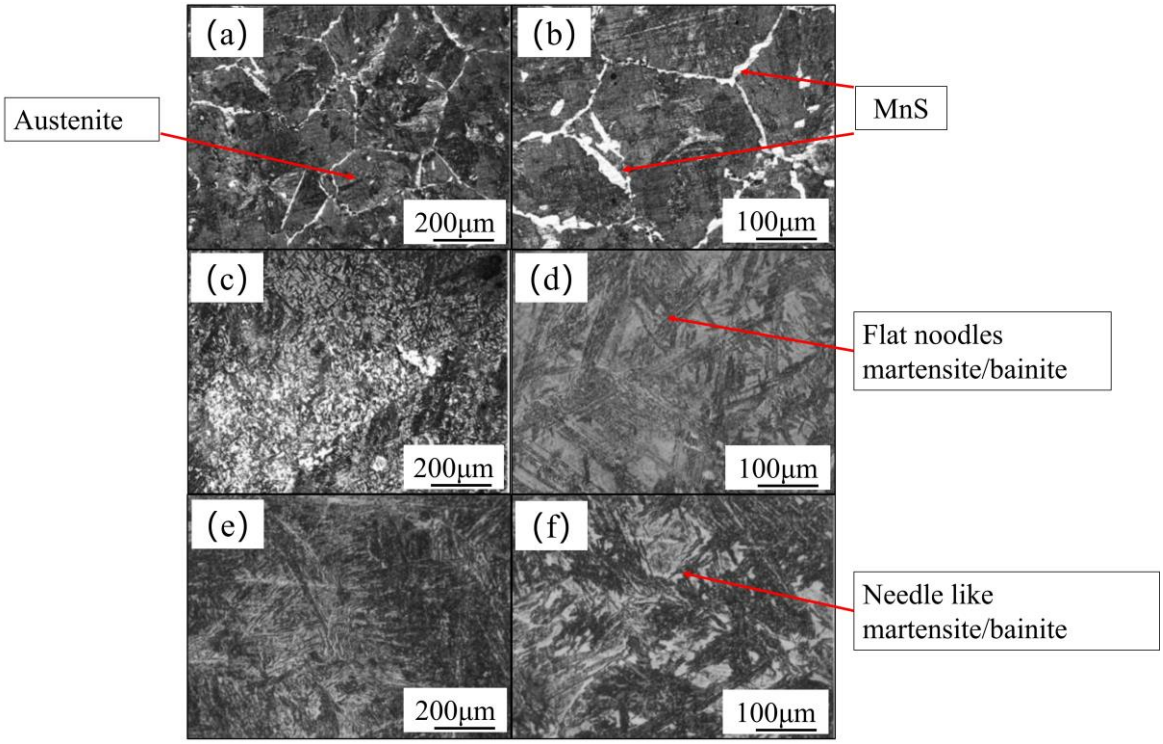

(a),(b).Furnace cooling; (c),(d).Air cooling; (e),(f).Water cooling

Figure 5. Morphology and distribution of sulfides at different cooling rates

Under furnace cooling conditions (Figure (a), (b)), a lower cooling rate allows the austenite grains to grow sufficiently, forming a coarse microstructure. At the same time, MnS inclusions tend to aggregate and coarsen at grain boundaries, forming distinct localized enrichment zones. The combined effect of coarse grain structure and inclusion segregation can easily lead to a decrease in material toughness and trigger transgranular fracture under stress.

Under air cooling conditions (Figure (c), (d)), faster cooling effectively inhibits austenite grain growth, significantly refines the structure, and generates a certain proportion of lath martensite/bainite duplex structure. Under this cooling system, the distribution of MnS inclusions tends to be uniform, and the degree of enrichment at grain boundaries is significantly reduced, which helps to improve the comprehensive mechanical properties of the material. In addition, faster cooling also suppresses the diffusion of impurity elements, further reducing the adverse effects of inclusions on performance.

Under water-cooled conditions (Figure (e), (f)), the extremely high cooling rate promotes further refinement of the microstructure, forming fine needle like martensite/bainite structures. Rapid cooling effectively suppresses the aggregation of MnS, reducing its size and making its distribution more uniform, which helps to improve the strength, toughness, and fatigue performance of the material. However, water cooling also leads to a significant increase in hardness and material brittleness, so tempering treatment is often required in engineering applications to achieve synergistic control of strength and toughness.

3.3. The relationship between secondary dendrites and cooling rate

A cotton swab dipped in a nitric acid aqueous solution of specific concentration was used to etch the specimen for 60 seconds. Following etching, the secondary dendrite morphology was observed and imaged using

 https://doi.org/10.64486/m.65.4.1

a scanning electron microscope (SEM). Subsequently, the secondary dendrite spacing (SDAS) was measured using Image software. Based on the empirical relationship between SDAS and cooling rate, the corresponding cooling rate values were calculated. The specific results are shown in Table 2.

Table 2. Secondary dendrite spacing measured under different cooling methods/μm

Furnace cooling	Air cooling	Water cooling
183	97	52

The relationship between secondary dendrite spacing and cooling rate is given by equations (1) and (2) [21].

$$\lambda_1=(169.1-720.9[C])\cdot R_c^{-0.4935},0<[C]<0.15\% \quad (1)$$

$$\lambda_2=143.9R_c^{-0.316}\cdot[C]^{(0.5501-1.996[C])},[C]>0.15\% \quad (2)$$

where:
λ - secondary dendrite spacing/μm;
Rc - cooling rate/(K/s).

Based on the actual chemical composition of the experimental steel, empirical formulas matching the carbon content were selected for calculation to obtain the cooling rates corresponding to different cooling methods. The results are shown in Table 3.

Table 3. Cooling rates corresponding to different cooling methods /K·s^{-1}

Furnace cooling	Air cooling	Water cooling
1.13	8.14	60.47

Based on the average diameter data of MnS inclusions in experimental steel at different cooling rates, a nonlinear fitting relationship between cooling rate and inclusion size was established. The mathematical expression is shown in equation (3), and the fitting curve is shown in Figure 6.

$$y = 6.8649\ x^{-0.184} \quad (3)$$

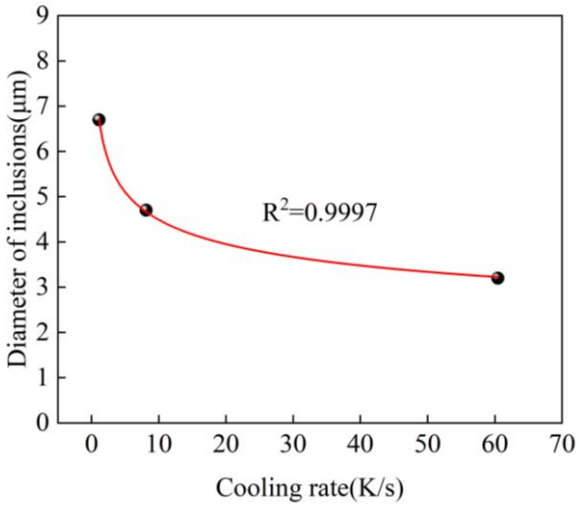

Figure 6. Fitting curve between cooling rate and inclusion diameter

https://doi.org/10.64486/m.65.4.1

4. Conclusions

(1) Under furnace cooling conditions, MnS inclusions significantly grow and precipitate along grain boundaries, leading to reduced material toughness and fatigue life; Under air-cooling conditions, MnS inclusion sizes are concentrated between (2–5) μm, exhibiting uniform morphology (aspect ratio approximately 2.0) and moderate number density (approximately 3.5/mm^2), which contributes to the optimization of comprehensive mechanical properties. Water-quenching treatment effectively refines MnS inclusions, enhancing the material's toughness and fatigue resistance.

(2) Cold quenching leads to coarse microstructure and MnS grain boundary segregation, causing performance degradation; water quenching yields an extremely fine microstructure with dispersed MnS, but its high hardness requires tempering; air quenching achieves microstructure refinement and uniform MnS distribution, offering the most optimal overall performance and representing the best process for achieving balanced properties.

(3) A nonlinear fitting relationship was established between the cooling rate and the average diameter of MnS inclusions, expressed as $y = 6.8649\ x^{-0.184}$.

Acknowledgments: Presented research was supported by the National Natural Science Foundation of China (52274334), the Hebei Provincial Innovation Capacity Enhancement Program (23561001D), the Hebei Provincial Natural Science Foundation (E2023209107), the Tangshan Municipal Science and Technology Bureau Key R&D Project (23150219A), and the Hebei Iron & Steel Group Key Science and Technology Project (HG2024124), Supported by the Graduate Student Innovation Fund of North China University of Science and Technology (2026B08).

References

[1] L. J. Su, T. Jun, S. Y. Hu, et al., "Effect of Ca/Mg on distribution and morphology of MnS inclusions in 45MnVS non-quenched and tempered steel," Metals, vol. 13, no. 1, pp. 23–34, 2023, https://doi.org/10.3390/met13010023

[2] Y. P. Wang, F. Z. Wang, W. B. Yu, et al., "Effects of MnS inclusions on mechanical behavior and damage mechanism of free-cutting steel: A molecular dynamics study," J. Mol. Graph. Model., vol. 118, Art. no. 108354, 2023, https://doi.org/10.1016/j.jmgm.2022.108354

[3] J. Y. Liu, C. S. Liu, R. J. Bai, et al., "Precipitation and growth of MnS inclusions in non-quenched and tempered steel under the influence of solute micro-segregations during solidification," Metall. Mater. Trans. B, vol. 52, no. 2, pp. 685–697, 2023, https://doi.org/10.1007/s11663-023-02718-3

[4] Q. R. Tian, N. F. Liu, W. Shen, et al., "Morphological differences of MnS inclusions in medium-carbon steel with different manganese and sulfur contents," Steel Res. Int., vol. 94, no. 9, Art. no. 2300074, 2023, https://doi.org/10.1002/srin.202300074

[5] C. K. Lin, Y. H. Su, W. S. Hwang, et al., "On pinning effect of austenite grain growth in Mg-containing low-carbon steel," Mater. Sci. Technol., vol. 34, no. 5, pp. 596–606, 2018, https://doi.org/10.1080/02670836.2018.1430171

[6] C. L. Xie, H. M. Zhang, G. Zhao, et al., "Effect of bismuth content and heating rate on MnS inclusions in free-cutting steel," Metals, vol. 14, no. 6, Art. no. 713, 2024, https://doi.org/10.3390/met14060713

[7] Q. Ren, L. Wang, Z. L. Xue, et al., "A thermodynamic assessment of precipitation, growth, and control of MnS inclusion in U75V heavy rail steel," High Temp. Mater. Process., vol. 40, no. 1, pp. 178–192, 2021, https://doi.org/10.1515/htmp-2021-0022

[8] H. Chu, L. Q. Zhang, J. Yang, et al., "Characterization of precipitation, evolution, and growth of MnS inclusions in medium/high manganese steel during solidification process," Mater. Charact., vol. 194, Art. no. 112367, 2022, https://doi.org/10.1016/j.matchar.2022.112367

[9] B. Xiao, H. Su, W. Ding, et al., "The influence of grinding parameters on the superficial hardening effect of 48MnV microalloyed steel," Key Eng. Mater., vols. 315–316, pp. 15–19, 2006, https://doi.org/10.4028/www.scientific.net/KEM.315-316.15

[10] L. Pan, R. Liu, Y. Wei, et al., "Austenite dynamic recrystallization of the microalloyed forging steels 38MnVS during forging process," Procedia Eng., vol. 27, pp. 63–71, 2011, https://doi.org/10.1016/j.proeng.2011.12.425

[11] N. Espinosa and J. Manuel, The Effect of Deoxidation Practice on Non-Metallic Inclusions and Their Effect on Mechanical Properties of a Low Alloy Steel, Ph.D. dissertation, Univ. Sheffield, Sheffield, U.K., 2018

[12] S. Bobba, B. H. Babu, M. S. Rao, et al., "The consequences of hot deformation and control cooling on the microstructure of medium carbon microalloyed steel–38MnSiVS5 grade". Mater Today, vol. 04, no. 290, pp. 2214-7853, 2023, https://doi.org/10.1016/j.matpr.2023.04.290

[13] Q. Y. Yu, X. G. Yang, C. B. Lai, et al., "Study on MnS inclusion aggregation along continuous casting slab thickness of medium carbon structural steel," Metals, vol. 12, no. 1, Art. no. 56, 2021, https://doi.org/10.3390/met12010056

[14] J. X. Liu, T. N. Peng, Z. W. Tian , et al., "Effect of cooling rate and Nb on the microstructure and hardness variation in microalloying medium-carbon non-quenched and tempered steel simulated in a die forging process," J Mater Eng and Perform., vol. 31, no. 8, pp. 6561-6571, 2022, https://doi.org/10.1007/s11665-022-06733-4

[15] L. Wang, C. Y. Zhu, J. Zeng, et al., "MnS precipitation behavior of high-sulfur microalloyed steel under sub-rapid solidification process," Metall. Mater. Trans. B, vol. 51, no. 1, pp. 45–53, 2020, https://doi.org/10.1007/s11663-019-01752-4

[16] J. Zeng, W. Q. Chen, and H. G. Zheng, "Analysis and control of central cracks in the bloom continuous casting of microalloy 49MnVS3 steel," Ironmaking Steelmaking, vol. 44, no. 9, pp. 676–684, 2017, https://doi.org/10.1080/03019233.2016.1228571

[17] S. W. Robinson, The Plastic Deformation of Non-Metallic Inclusions in Steel, Sheffield Hallam Univ., Sheffield, U.K., 1977

[18] J. Yamamoto, H. Yamamura, Y. Suuwa, et al., "Behavior of non-metallic inclusions in steel during hot deformation and the effects of deformed inclusions on local ductility," ISIJ Int., vol. 51, no. 12, pp. 1987–1994, 2011, https://doi.org/10.2355/isijinternational.51.1987

[19] X. R. Bi, Z. Y. Hu, L. Xing, et al., "Effect of cooling method on microstructure and hardness of 20CrMnSi steel after flame cutting," Mater. Rev., vol. 38, no. 1, pp. 487–490, 2024

[20] H. Li, F. X. Wang, X. Y. Fang, et al., "Effect of cooling method on microstructure and mechanical properties of 45CrNiMoVA high strength steel," J. Metal Heat Treat., vol. 49, no. 2, pp. 215–220, 2024, https://doi.org/10.13251/j.issn.0254-6051.2024.02.034

[21] W. Yang, X. G. Yang, L. F. Zhang, et al., "Summary of MnS inclusion control in steel," Steelmaking, vol. 29, no. 6, pp. 71–78, 2013